 DOI: 10.1002/masy.200651338

Computer Simulations of Polyelectrolyte Stars Near Walls

Martin Konieczny, Christos N. Likos

Summary: We present results from monomer-resolved, Molecular Dynamics computer simulations of multiarm, star-shaped polyelectrolytes brought in the vicinity of planar, uncharged walls. We demonstrate that polyelectrolyte stars are very robust against planar confinement, in the sense that they maintain their key properties from the bulk, despite their strong deformation due to the wall: the chains remain stretched, the radius is insensitive to the wall and the number of trapped counterions is barely affected by the wall. We supplement our study with measurements of the star-wall force and a corresponding analytic theory.

Keywords: charged systems; computer simulations; polyelectrolytes

I. Introduction

One of the most interesting, both theoretically and technologically, types of macromolecules are polyelectrolytes (PE's). These are polymer chains that carry ionizable groups along their backbones, which lose their counterions via dissociation upon dissolution in a polar solvent (water). PE's combine aspects of chain connectivity and electrostatics, thus displaying a richness of conformations and physical states that greatly exceeds that of neutral polymer chains. The situation becomes even more interesting if one now chemically attaches f linear polyelectrolyte chains on a rigid particle of radius R_d. One then speaks of a spherical PE-brush (planar brushes result by grafting on flat walls). In the limit in which the height of the brush greatly exceeds R_d, PE-stars result, the topic of the current contribution. A great deal of theoretical[1–17] and experimental[18–27] work has been devoted to the study of spherical brushes and stars in the recent past, due to the importance of the grafted chains in colloidal stabilization but also as a result of the interest in PE-stars as novel, soft and controllable colloidal aggregates. Effective interactions between PE-stars have been derived and some of the theoretical predictions on their structural and phase behavior[8,11] have been experimentally confirmed.[28]

As far as the properties of single stars in low concentrations are concerned, the most striking feature they show is their ability to act as trapping agents for their own counterions, readsorbing and recondensing in their interior as much as 90% of the counterions they release.[1,4,5,7,8] This happens when the chains are stretched and such PE-stars are called *osmotic*. A novel field of intriguing physics is arising when PE-stars are mixed with hard colloids or brought in contact with planar walls, due to their promising applications as drug-delivery and protein-encapsulation and immobilization agents[29–32] or as building blocks of tunable microlenses.[33–36] It is therefore pertinent to examine the conformations of PE-stars close to walls in order to determine to which extent a wall affects the self-organization of the star and its accompanying counterions. In this work, we present computer simulation results regarding the shapes and properties of PE-stars close to planar,

Institut für Theoretische Physik II: Weiche Materie, Heinrich-Heine-Universität Düsseldorf, Universitätsstraße 1, D-40225 Düsseldorf, Germany

Paper presented as invited contribution at the **IUPAC-Macro 2006 Conference**, July 17–21, 2006, Rio de Janeiro, Brazil. Submitted for publication in *Macromolecular Symposia*.

neutral walls as well as the effective forces that develop when PE-stars are brought in close contact with such planar surfaces.

II. Simulations of Free Polyelectrolyte Stars

We construct the PE-stars by considering f PE-chains that are all attached to a common core of radius R_d. In order to be indeed in the star-burst limit, we choose the latter to have a size similar to the monomer length, to be defined below. Due to reasons of overcrowding in the middle of the star, a finite value of R_d is necessary. The PE-chains themselves are modeled in a coarse-grained fashion, i.e., atomistic details are not taken into consideration. Instead, the chains are regarded as bead-spring sequences of N Lennard-Jones (LJ) monomers, an approach broadly employed also for the computer modeling of neutral polymer chains and stars[37–39] and of linear polyelectrolytes.[40] We consider good solvent conditions without explicit solvent, thus the monomer-monomer interaction has to be purely repulsive. To this end, a shifted and truncated LJ potential is employed that reads as:

$$V_{\mathrm{LJ(r)}} = \begin{cases} 4\varepsilon_{\mathrm{LJ}}\left[\left(\frac{\sigma_{\mathrm{LJ}}}{r}\right)^{12} - \left(\frac{\sigma_{\mathrm{LJ}}}{r}\right)^{6} + \frac{1}{4}\right] & \mathrm{r} \le 2^{1/6}\sigma_{\mathrm{LJ}} \\ 0 & \mathrm{r} > 2^{1/6}\sigma_{\mathrm{LJ}} \end{cases} \quad (1)$$

In Eq. (1) above, r denotes the distance of two monomers. The quantity σ_{LJ}can be identified with the monomer size and sets the length scale of the problem, whereas $\varepsilon_{\mathrm{LJ}\sigma}$ is the energy scale. The temperature is fixed at the value $T = 1.2\ \varepsilon_{\mathrm{LJ}}/k_B$, where k_B denotes Boltzmann's constant. Bonding between sequential monomers is modeled by the finite extension nonlinear elastic (FENE) potential:[38,39]

$$V_{\mathrm{FENE}}(r) = \begin{cases} -\frac{k_{\mathrm{FENE}}}{2}\left(\frac{R_0}{\sigma_{\mathrm{LJ}}}\right)^2 \mathrm{In}\left[1 - \left(\frac{r}{R_0}\right)^2\right] & r \le R_0 \\ \infty & r > R_0, \end{cases} \quad (2)$$

with a spring constant $k_{\mathrm{FENE}} = 7.0\varepsilon_{\mathrm{LJ}}$. The divergence length R_0 limits the maximum relative displacement of two neighboring monomers and is set to $R_0 = 2.0\sigma_{\mathrm{LJ}}$. The equilibrium bond length results from the position of the minimum of the sum of the steric and bonding interactions and has, in this case, the value $l_0 = 0.97\sigma_{\mathrm{LJ}}$. The bonding of the initial monomers that are grafted on the core are modeled in a similar way, taking into account the central particle's radius R_d. Thus, we have for the grafting the sum of a steric potential $V^c_{\mathrm{LJ}}(r)$ and a FENE-potential $V^c_{\mathrm{FENE}}(r)$ of the form:

$$V^c_{\mathrm{LJ}} = \begin{cases} \infty & r \le R_d \\ V_{\mathrm{LJ}}(r - R_d) & \mathrm{r} > \mathrm{R_d} \end{cases} \quad (3)$$

and

$$V^c_{\mathrm{FENE}} = \begin{cases} \infty & r \le R_d \\ V_{\mathrm{FENE}}(r - R_d) & r > R_d. \end{cases} \quad (4)$$

We charge *every* (l/α)-th monomer ($\alpha < 1$) along the chain by assigning to it an elementary charge e, introducing at the same time a total of $N_c = \alpha\, Nf$ counterions of opposite charge, - e, where N is the degree of polymerization of each chain. The counterion-charged monomer as well as the counterion-counterion interactions also include a steric, short-range repulsion given by Eq. (1) above. This is particularly important for stability, since attractive Coulomb interactions between oppositely charged point-particles lead to a collapse of the two onto each other.

Finally, we have to introduce the interactions between the charged components, which are simply given by the Coulomb potential

$$\beta V^{ij}_{\mathrm{Coul}}(r) = \beta \frac{q_i q_j e^2}{er} \equiv \lambda_B \frac{q_i q_j}{r}. \quad (5)$$

Here, $q_i, q_j = \pm 1$ are the valencies of monomer ions and counterions, respectively, ($\beta = 1/(k_B T)$ and e is the dielectric constant of the solvent. The Bjerrum length

$$\lambda_B = \frac{\beta e^2}{\varepsilon} \quad (6)$$

denotes as the distance at which the electrostatic energy equals the thermal

energy and provides a measure for the strength of the Coulomb coupling. For water ($e = 80$) at $T = 300$ K, we have $\lambda_B = 7.1$ Å; in terms of the unit of length, σ_{LJ}, we fixed the ratio $\lambda_B/\sigma_{LJ} = 3.0$, corresponding to a realistic[41] monomer size $\sigma = 2.4$ Å.

In Fig. 1 we show a typical simulation snapshot of a PE-star with $f = 30$ arms and $\alpha = 1/3$, far away from the confining walls, i.e., free of their influence. It can be seen that the star arms are stretched and that the vast majority of the counterions are within the sphere delineated by the star extension. This is a manifestation of the property of PE-stars to 'trap' in their interior the counterions that they release. Suppose now that the PE-star is brought very close to the wall shown at the bottom of Fig. 1. The volume in the star's interior will be halved, due to the loss of the half-space taken by the bottom side of the wall. Thus, the trapped counterions will lose entropy and it is reasonable to assume that a good fraction of them will be released into the solution. Further, the planar confinement may bring about more drastic, conformational changes, such as chain stretching or collapse. The investigation of the shape that the PE-star assumes under such conditions is the subject of the following section.

III. Simulations of Confined Polyelectrolyte Stars

We now additionally introduce two neutral, hard walls parallel to the x-y-plane at positions $z = \pm\tau/2$, resulting in an overall wall-to-wall separation τ. In principle, the discontinuity of the dielectric constant on the two sides of the planar wall implies the necessity to introduce image charges. However, we do not expect the latter to have a significant impact on the conformation of that star, since the overall charge of the latter is drastically reduce due to the presence of the adsorbed counterions, thus we neglect image charges in what follows.

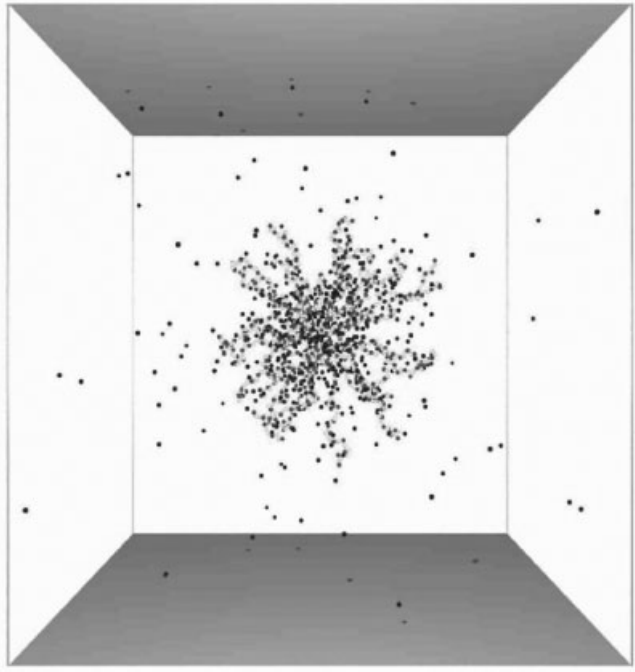

Figure 1.
A polyelectrolyte star with $f = 30$ arms away from the confining walls, demonstrating the star's conformation. The dark, free spheres are the counterions. The light monomers along the chains are neutral and the dark ones are charged.

The wall-particle interaction is purely repulsive and short-range. In parallel lines with the modeling of monomers as Lennard-Jones spheres, and based on Eq. (1), we introduce a truncated-and-shifted LJ interaction between the wall and the monomers, which is also identical to the wall-counterion potential and reads as:

$$V_{\mathrm{LJ}}^{\mathrm{w}}(z) = V_{\mathrm{LJ}}\left(\frac{T}{2} - z\right) + V_{\mathrm{LJ}}\left(\frac{T}{2} + z\right), \qquad (7)$$

whereas z refers to the z-component of the position vector of the particular particle (monomer or counterion). The finite-size central core interacts with the wall by a similar potential, shifted by R_{d} i.e.:

$$V_{\mathrm{LJ}}^{\mathrm{wc}}(z) = V_{\mathrm{LJ}}\left(\frac{T}{2} - R_{\mathrm{d}} - z\right) + V_{\mathrm{LJ}}\left(\frac{T}{2} - R_{\mathrm{d}} + z\right). \qquad (8)$$

IV. Results

The PE-star is enclosed in a rectangular simulation box of total volume $V = \tau\ M^2$, with periodic boundary conditions applied in the x- and y-directions, while the box is confined with respect to the z-direction. Here, we always fix $M = \tau = 120\sigma_{\mathrm{LJ}}$. The equations of motion were integrated numerically using the Verlet algorithm in its velocity form,[42–44] whereas a Langevin thermostat[42–44] was employed to stabilize the system's temperature. The long-range Coulomb interaction was taken into account for its two-dimensional periodicity by modifying Lekner's summation technique[45] in two dimensions. We considered three different functionalities, $f = 10$, $f = 18$ and $f = 30$, three different charging fractions, $\alpha = 1/5$, $\alpha = 1/4$, and $\alpha = 1/3$ and a single degree of polymerization per chain, $N = 50$. For every different distance D between the star center and the planar wall, the system was equilibrated for about 5×10^5 time steps and we performed production runs lasting between 1×10^6 and 2×10^6 time steps.

In Fig. 2 we show a simulation snapshot of a $f = 18$, $\alpha = 1/3$ PE-star very close to the planar wall and in Fig. 3 the same for a $f = 30$, $\alpha = 1/3$ PE-star. It can be seen, also in comparison with Fig. 1 that although the PE-star is strongly deformed by the wall presence, still the great majority of counterions remains trapped in its interior. Moreover, no significant shrinkage or expansion of the PE-star can be noticed. In order to quantify these assertions, we have measured in our simulation a number of quantities of interest that we list below.

1. The Star Radius

Here, we have monitored the center-to-end distance R of every chain and averaged over all chains for any given separation D between the star center and the wall. In particular, we measure the quantity,

$$R(D) = \sqrt{\frac{1}{f}\left\langle \sum_{i=1}^{f} (\mathrm{r}_{i,N} - \mathrm{r}_{\mathrm{core}})^2 \right\rangle_D}, \qquad (9)$$

where $r_{\mathrm{i},N}$ denotes the position of the end-monomer of the i-th chain and $\mathbf{r}_{\mathrm{core}}$ the core position. The angular brackets $<\bullet\ \bullet\ \bullet>_D$ stand for the statistical average, which is taken for any *fixed* value of the star-to-wall distance D. In Fig. 4 we show the measured spatial extent $R(D)$ for stars with functionalities $f = 10$, $f = 18$, and $f = 30$. In all cases, the charging fraction is chosen to be $\alpha = 1/3$. It can be seen that the radii are hardly affected by the distance D to the wall, even when the latter changes from a value between two and three star radii (free star) to zero. Due to the chain stretching, the star is thus *robust* against confinement, as far as its size is concerned. It should also be noticed that the radii are practically independent of the arm number f, in contrast to the case of neutral stars, for which a scaling law $R \sim f^{1/5}$ holds.[46]

Looking at the results in more detail, we can discern a slight depression of the arm-averaged star radius that starts at distance $D_{\max} \cong 1.3R$, where R denotes the radius of the free star. This effect stems

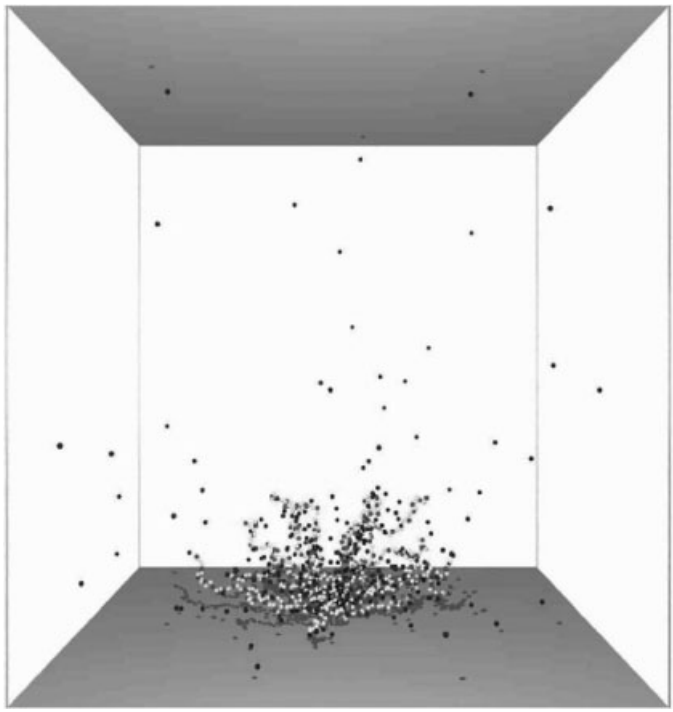

Figure 2.
Simulation snapshot of a polyelectrolyte star with $f = 18$ arms close to the confining wall.

from a compression mechanism of a few chains of the star as the latter approaches the wall. The compression reaches its strongest extent at distances $0.7\,R \lesssim D_0 \lesssim 0.9\,R$ and thereafter the chains are getting released and decompressed, slipping tangentially to the wall, as sketched in Fig. 5 that follows. This mechanism gives also a contribution to the effective star-wall force, as will be discussed in the following section.

2. Condensed Counterions

When strongly charged polyelectrolytes are present, there are two kinds of counterion capturing that can take place: strong, or Manning condensation[47–49] and weak trapping. The former refers to the fact that a certain fraction of the released counterions physisorbs in the neighborhood of the release sites, forming tightly-bound ion pairs. We expect, thus, that a certain number N_1 of the counterions will be found within a distance λ_B from the monomer ions, being confined to move in narrow cylinders around the stretched, rodlike chains. In order to monitor the Manning-condensed counterions along the simulation, we surrounded each charged monomer by a fictitious sphere of radius λ_B and counted the number of counterions in every sphere, performing time averages along the MD-run for every star-wall separation D. The quantity N_1 depends, of course, on the charging fraction α and on the functionality f, however it is practically independent on D, as Fig. 6 demonstrates. For this type of condensation effect, electrostatics is dominating and confinement cannot affect the ability of the PE-star to Manning-condense a significant fraction of the counterions.

3. Trapped Counterions

In addition to the Manning-condensed counterions, there is also an additional number N_2 of them, which remains confined in the sphere of radius R formed by the

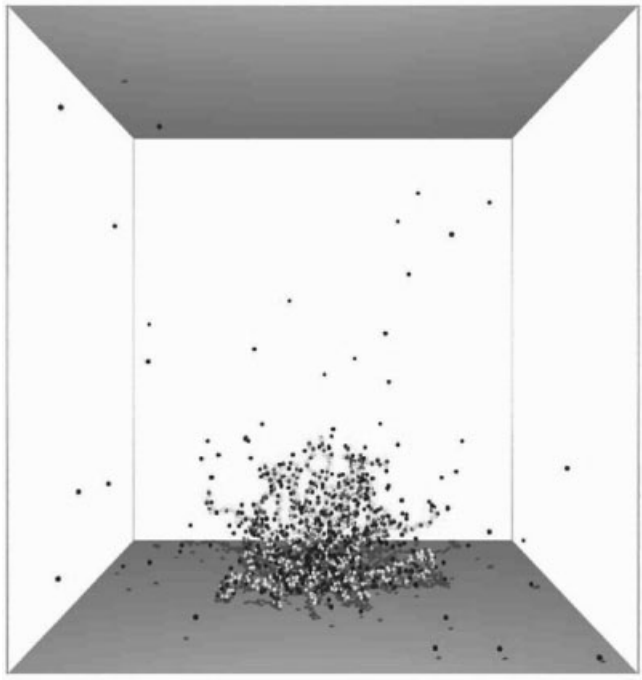

Figure 3.
Same as Fig. 2 but for a $f = 30$-arm star.

brush, without becoming strongly condensed along the chains. These still have the freedom to move inside the sphere but they cannot leave its interior and they are called *spherically condensed* or *weakly trapped*. In the simulation, we measured the total number of counterions present within a sphere of radius R equal, in every

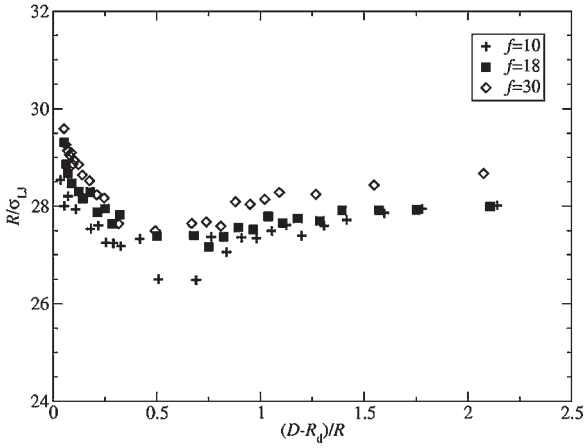

Figure 4.
The star radii as a function of the star-wall distance for fixed charging fraction $\alpha = 1/3$ but for different functionalities f as indicated in the legend. Note that the stars' spatial extensions are almost independent on D. Moreover, the radii are only weakly affected by the functionality.

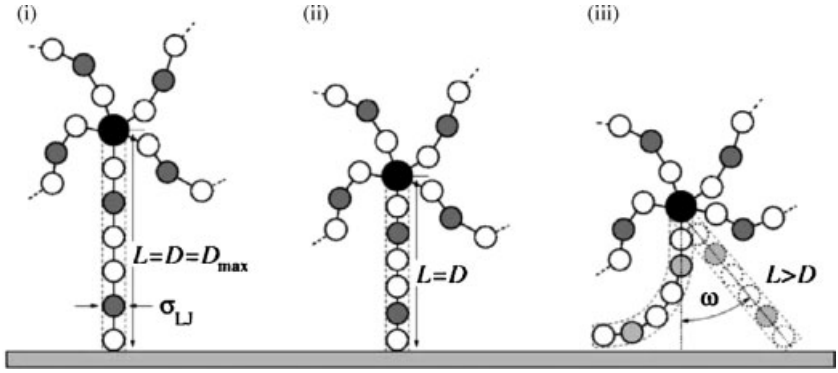

Figure 5.
A sketch of the compression-decompression mechanism of the arms of the PE-star that are oriented perpendicular to the wall as the former approaches the latter. In (i), the arm has just touched the wall and still has its maximum extension $L = D_{max} = 1.3R$. In (ii), $L < D_{max}$ the chain compresses and $L = D$. This persists down to a star-wall distance D_o; when $D < D_o$, as in (iii), the compression cost becomes too high, so the chain bends, as sketched by the rod bent to the left. For the purposes of theoretical modelling, we have replaced the bent rod with a straight one of the same center-to-end distance, and the latter is depicted mirror-reflected to the right to avoid crowding.

measurement step, to the average between the instantaneous center-to-end distances of all f chains. The procedure was carried out for every distance D from the wall. In Fig. 7 we show the dependence of the total number of trapped counterions, $N_{in} = N_1 + N_2$ on the star-wall separation D. We see once more that this number is practically independent of the proximity of the planar wall. Thus, we have established that PE-stars are simultaneously flexible and robust objects. They undergo drastic deformations upon close approach to a hard, planar, repulsive wall, halving the space available in their interior when their center approaches the wall to distances of the

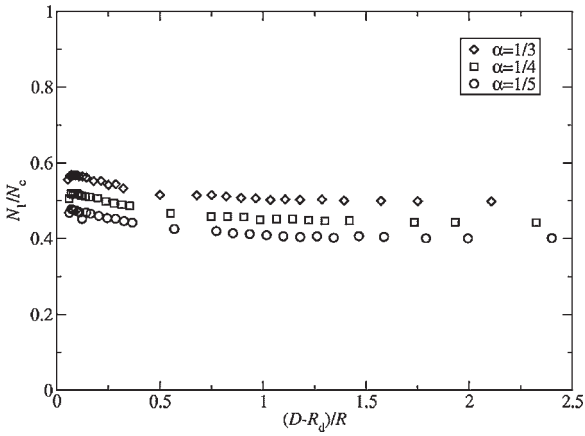

Figure 6.
The fraction N_1/N_c of strongly condensed counterions for $f = 18$ PE-stars and for various charging fractions α, indicated in the legend, as a function of the star-wall distance. Note the insensitivity of N_1/N_c on D.

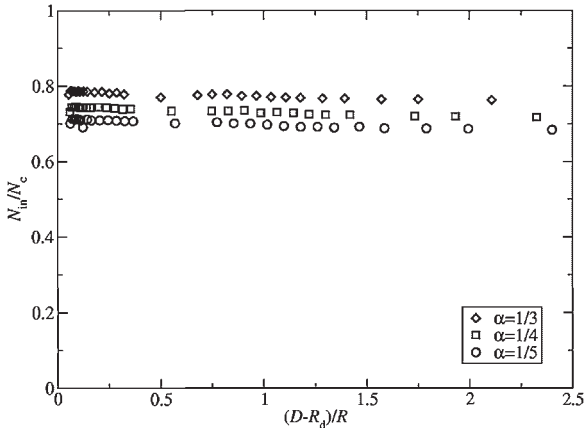

Figure 7.
Same as Fig. 6 but for the total number of counterions N_{in} trapped in the interior of $f = 18$ PE-stars.

order of a monomer length. Despite of this fact, neither their radius nor their ability to strongly capture the vast majority of their counterions is affected by this confinement. The results of our investigations regarding the radius and the number of trapped counterions are summarized in Table 1.

V. The Effective Star-Wall Force

An additional quantity of great interest is the effective force that is experienced by the center of the star as it approaches the wall. There are several contributions to this force: the D-dependence of the total electrostatic energy of the star and its counterions due to the change of the star shape, $V_{es}(D)$; the loss of entropy of the trapped counterions, $V_{entr}(D)$, due to the decrease of the available volume in the interior of the star; and, finally, the aforementioned compression mechanism of isolated chains, giving rise to an additional potential $V_{comp}(D)$. The three terms add to the effective star-wall potential, $V_{eff}(D)$:

$$V_{eff}(D) = V_{es}(D) + V_{entr}(D) + V_{comp}(D). \quad (10)$$

The magnitude of the effective force is then given as the gradient of $V_{eff}(D)$, i.e.,

$$F_{eff}(D) = -\frac{\partial V_{eff}(D)}{\partial D}. \quad (11)$$

For a detailed discussion of the terms $V_{es}(D)$ and $V_{entr}(D)$, we refer the reader to Ref. 51. Here, we proceed with a concise presentation of the compression contribution $V_{comp}(D)$ and the way it was modeled in theory.

As discussed in the preceding section, for D in the order of the typical length of an arm of the star, the star will undergo strong configurational variations to avoid the wall since the monomers are not able to interpenetrate it. Thereby, due to the presence of neighboring arms, it can be energetically favorable for chains directing towards the wall to compress instead of bending away from the surface, although this compression leads to an extra cost in electrostatic energy. Based on simulation data, we therefore make the following assumption for the dependence of the length of those chains that face the wall perpendicularly on D, in conjunction with Fig. 5. If the separation becomes smaller than $D_{max} = 1.3\,R$, the chains start compressing and the chain length $L = D$ down to a distance $D_0 = 0.9\ R$. Further compression causes the chain to bend/slip and the length

Table 1.
Conformational properties as obtained from MD simulations for different arm numbers and charging fractions. In addition, results from Ref. 8 are presented for comparison. The chain length is fixed to $N = 50$. Note that there are in part insignificant discrepancies between the parameters used here and in Ref. 8.

f	α	N_c	$(R/\sigma_{LJ})^{a)}$	$(N_1)^{a)}$	$(N_{in})^{a)}$	$(R/\sigma_{LJ})^{b)}$	$(N_1)^{b)}$
10	1/5	100	24.0	32	60	–	–
10	1/4	120	24.8	44	78	25.3	46
10	1/3	170	27.5	76	122	27.4	72
18	1/5	180	24.6	78	126	–	–
18	1/4	216	25.4	104	159	26.6	107
18	1/3	306	28.0	163	238	28.3	159
30	1/5	300	25.1	161	229	–	–
30	1/4	360	25.9	208	284	27.2	213
30	1/3	510	28.4	315	418	28.6	309

a) Values as obtained from our MD simulations, averaged with respect to D.
b) Simulation results for isolated PE-stars, taken from Ref. 8, shown for comparison.

L correspondingly starts increasing again: $L = 2D_0 - D$, until a minimum distance $D_{min} = 0.5\ R$ is reached, at which point the chain retains its original, undisturbed length. In mathematical terms, thus

$$L(D) = \begin{array}{cc} D_{max} & D \in [0, D_{min}[\\ 2D_0 - D & D \in [D_{min}, D_0[\\ D & D \in [D_0, D_{max}[\\ D_{max} & D \in [D_{max}, \infty[. \end{array} \qquad (12)$$

This D-dependence of the length of the compressed chains brings about an energetic penalty, since the rods can be viewed as elastic springs of equilibrium length D_{max} and spring constant k_{eff}. The latter can be calculated from the sum of electrostatic and elastic energies of a uniformly charged rod[50] with linear charge density η:

$$\begin{aligned} \beta U_{rod}(L) &= \beta U_{elec}(L) + \beta U_{elas}(L) \\ &= \beta \tfrac{\eta^2}{\varepsilon} L \ln\left(\tfrac{L}{\sigma_{LJ}}\right) - \tfrac{\beta k_{eff}}{2} L^2 \\ &= \tfrac{Z^2\alpha^2 N^2 \lambda_B}{L} \ln\left(\tfrac{L}{\sigma_{LJ}}\right) - \tfrac{\beta k_{eff}}{2} L^2 \end{aligned} \qquad (13)$$

by setting $\partial U_{rod}/\partial L|_{L=D_{max}} = 0$. Accordingly, when $L(D) \neq D_{max}$, a compression contribution to the force is obtained as

$$F_{comp}(D) = \begin{cases} -f_c \frac{D}{L(D)} \frac{\partial U_{rod}}{\partial L} | L = L(D) & D \in [D_{min}, D_{max}] \\ 0 & \text{otherwise.} \end{cases} \qquad (14)$$

Here, f_c is the total number of compressed chains, in general a small fraction of f. Assuming that the chains are regularly attached to the colloidal core, we expect a linear relation between f_c and f, namely $f_c = f/f_0$. Simulation data indicate $f_0 = 4$ to be a good choice for all parameter combinations under investigation. The pre-factor $D/L(D) = \cos\omega$ results from geometrical considerations, as can be seen from Fig. 5. Based on Eq. (14), we obtain the corresponding energy term $V_{comp}(D)$ by a simple integration:

$$V_{comp}(D) = \int_{\infty}^{D} F_{comp}(D')dD'. \qquad (15)$$

The theoretical model must be tested against MD measurements. Keeping the star center at a fixed position $\mathbf{r}_{core}$ as effective coordinate in our simulations, the effective force $\mathbf{F}(\mathbf{r}_{core})$ can be measured as the time average over all instantaneous, microscopic forces $\mathbf{f}_{core}$ acting on the core, namely

$$\mathrm{F}(\mathrm{r}_{core}) = \langle \mathrm{f}_{core} \rangle. \qquad (16)$$

Due to symmetry, $F_{core}(\mathbf{r}_{core}) = |\mathbf{F}_{core}(\mathbf{r}_{core})|$ will only have a z-component and will depend on the z-coordinate of r_{core}, namely on D. The theoretical treatment is successful if the relation

$$F_{core}(D) = F_{eff}(D) = -\frac{\partial V_{eff}(D)}{\partial D}. \qquad (17)$$

holds to a satisfactory degree of approximation.

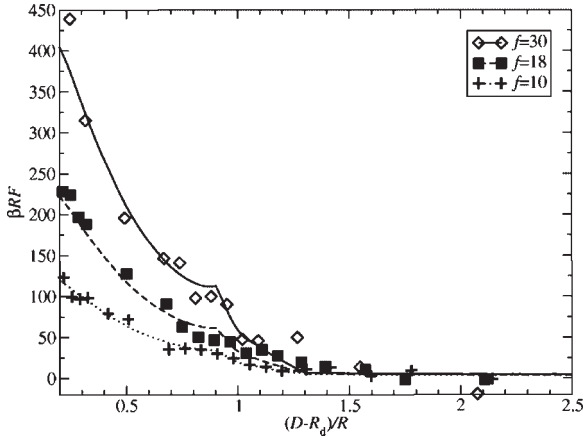

Figure 8.
Effective forces between PE-stars and planar walls as functions of the star-wall distance *D*. Here, results for three different functionalities are shown, as indicated in the legend, whereas the charge fraction is kept fixed at $\alpha = 1/3$. Symbols: simulation results; lines: theory.

Representative results, comparing theory and simulation are shown in Fig. 8, where it can be seen that theory indeed captures the measured force in a quantitative fashion. The main contribution to the effective force arises from the entropy loss of the trapped coun-terions. Nevertheless, this alone (and the much weaker electrostatic contribution) cannot correctly account for the additional repulsive 'shoulder' of the force curves seen in the region $0.5 \lesssim D/R \lesssim 1.3$. This is precisely the contribution arising from the compression mechanism, which makes itself therefore manifest not only in the slight decrease of the average star radius there but also in a visible and important contribution to the effective star-wall force. Additional corroboration for the presence of this novel repulsion mechanism is offered by the fact that such forces are *absent* between two PE-stars. There, the entropic and electrostatic contributions are fully adequate to account for the characteristics of the measured force,[7,8] because the chain compression is an effect present only when the stars encounter impenetrable objects, such as planar or curved walls. On a quantitative basis, we note that, as expected, the force is repulsive and soft; moreover, its magnitude grows with the functionality f since this implies that a larger number of trapped counterions is entropically punished and a larger number of chains is compressed. In fact, a rough scaling $F(D) \sim f$ can be discerned.

VI. Conclusions

Computer simulations provide an indispensable tool for the study of the properties of complex macromolecules. They allow for the construction of well-defined models and the isolation of physical mechanisms that are usually hard to control in experiments, due to the influence of various obscuring factors (imperfections at the synthesis, polydispersity, system impurities etc.) In this contribution, we analyzed by means of Molecular Dynamics simulations the conformations of multiarm polyelectrolyte stars in the proximity of planar, uncharged walls. We have established that these soft colloids are surprisingly robust against confinement: although they do deform to fit their new local environment, they do maintain their size and they continue to act as super-absorbers for the counterions. It appears then, that if one wants to manipulate PE-stars in a more drastic way, force them to achieve collapsed configurations or release their counterions fully, one has to apply to them stronger external influences.

A very promising perspective is offered by using *charged* planar walls with a tunable surface charge density (e.g., placing them between the plates of a planar capacitor or close to an ionizable surface). Results from this line of research will be the topic of future publications.

Acknowledgements: The authors wish to thank Dr. Arben Jusufi (Princeton University) for helpful discussions.

[1] P. Pincus, *Macromolecules* **1991**, *24*, 2912.
[2] J. Klein Wolterink, J. van Male, M. A. Cohen Stuart, L. K. Koopal, E. B. Zhulina, O. V. Borisov, *Macromolecules* **2002**, *35*, 9176.
[3] J. Klein Wolterink, F. A. M. Leermakers, G. J. Fleer, L. K. Koopal, E. B. Zhulina, O. V. Borisov, *Macromolecules* **1999**, *32*, 2365.
[4] O. V. Borisov, E. B. Zhulina, *J. Phys. II* **1997**, *7*, 449.
[5] O. V. Borisov, E. B. Zhulina, *Eur. Phys. J. B* **1998**, *4*, 205.
[6] N. P. Shusharina, P. Linse, A. R. Khokhlov, *Macromolecules* **2000**, *33*, 3892.
[7] A. Jusufi, C. N. Likos, H. Löwen, *Phys. Rev. Lett.* **2002**, *88*, 018301.
[8] A. Jusufi, C. N. Likos, H. Löwen, *J. Chem. Phys.* **2002**, *116*, 11011.
[9] A. R. Denton, *Phys. Rev. E* **2003**, *67*, 011804; Erratum, *ibid. 67*, **2003**, 011804 (E).
[10] H. Wang, A. R. Denton, *Phys. Rev. E* **2004**, *70*, 041404.
[11] N. Hoffmann, C. N. Likos, H. Löwen, *J. Chem. Phys.* **2004**, *121*, 7009.
[12] A. Jusufi, C. N. Likos, M. Ballauff, *Colloid Polym. Sci.* **2004**, *282*, 910.
[13] M. Roger, P. Guenoun, F. Muller, L. Belloni, M. Delsanti, *Eur. Phys. J. E* **2002**, *9*, 313.
[14] O. V. Borisov, E. B. Zhulina, *Macromolecules* **2002**, *35*, 4472.
[15] E. B. Zhulina, O. V. Borisov, *Macromolecules* **2002**, *35*, 9191.
[16] O. V. Borisov, E. B. Zhulina, *Macromolecules* **2003**, *36*, 10029.
[17] A. Jusufi, *J. Chem. Phys.* **2006**, *124*, 044908.
[18] P. Guenoun, F. Muller, M. Delsanti, L. Auvray, Y. J. Chen, J. W. Mays, M. Tirrell, *Phys. Rev. Lett.* **1998**, *81*, 3872.
[19] W. Groenewegen, S. U. Egelhaaf, A. Lapp, J. R. C. van der Maarel, *Macromolecules* **2000**, *33*, 3283.
[20] W. Groenewegen, A. Lapp, S. U. Egelhaaf, J. R. C. van der Maarel, *Macromolecules* **2000**, *33*, 4080.
[21] J. R. C. van der Maarel, W. Groenewegen, S. U. Egelhaaf, A. Lapp, *Langmuir* **2000**, *16*, 7510.
[22] T. Abraham, S. Giasson, J. F. Gohy, R. Jérôme, *Langmuir* **2000**, *16*, 4286.
[23] Q. de Robillard, X. Guo, M. Ballauff, T. Narayanan, *Macromolecules* **2000**, *33*, 9109.
[24] X. Guo, M. Ballauff, *Phys. Rev. E* **2001**, *64*, 051406.
[25] N. Dingenouts, R. Merkle, X. Guo, T. Narayan, G. Goerick, M. Ballauff, *J. Appl. Crystal-logr* **2003**, *36*, 578.
[26] M. Heinrich, M. Rawiso, J. G. Zilliox, P. Lesieur, J. P. Simon, *Eur. Phys. J. E* **2001**, *4*, 131.
[27] A. V. Korobko, W. Jesse, S. U. Egelhaaf, A. Lapp, J. R. C. van der Maarel, *Phys. Rev. Lett.* **2005**, *93*, 177801.
[28] T. Furukawa, K. Ishizu, *Macromolecules* **2005**, *38*, 2911.
[29] G. Riess, *Prog. Polym. Sci.* **2003**, *28*, 1107.
[30] S. R. Bhatia, A. Mourchid, M. Joanicot, *Curr. Opin. Colloid Interface Sci.* **2001**, *6*, 471.
[31] Y. Kakizawa, K. Kataoka, *Adv. Drug. Deliv. Rev.* **2002**, *54*, 203.
[32] P. M. Biesheuvel, A. Wittemann, *J. Phys. Chem. B* **2005**, *109*, 4209.
[33] J. Kim, M. J. Serpe, L. A. Lyon, *J. Am. Chem. Soc.* **2004**, *126*, 9512.
[34] M. J. Serpe, J. Kim, L. A. Lyon, *Adv. Mater* **2004**, *16*, 184.
[35] J. Kim, M. J. Serpe, L. A. Lyon, *Angew. Chem. Int. Ed.* **2005**, *44*, 1333.
[36] J. Kim, S. Nayak, L. A. Lyon, *J. Am. Chem. Soc.* **2005**, *127*, 9588.
[37] M. J. Stevens, K. Kremer, *Phys. Rev. Lett.* **1993**, *71*, 2228.
[38] G. S. Crest, K. Kremer, T. A. Witten, *Macromolecules* **1987**, *20*, 1376.
[39] G. S. Crest, *Macromolecules* **1994**, *27*, 3493.
[40] M. Konieczny, C. N. Likos, H. Löwen, *J. Chem. Phys.* **2004**, *121*, 4913.
[41] W. Essafi, F. Lafuma, C. E. Williams, *J. Phys. II (France)* **1995**, *5*, 1269.
[42] M. P. Allen, D. J. Tildesley, *Computer Simulation of Liquids*, Oxford University Press, Oxford, **1987**.
[43] D. Frenkel, B. Smit, *Understanding Molecular Simulation*, Academic Press, San Diego, **1996**.
[44] D. C. Rapaport, *The Art of Molecular Dynamics Simulation*, Cambridge University Press, Cambridge, **1995**.
[45] J. Lekner, *Physica A* **1991**, *176*, 485.
[46] C. N. Likos, *Phys. Rep.* **2001**, *348*, 267.
[47] G. S. Manning, *J. Chem. Phys.* **1969**, *51*, 924.
[48] G. S. Manning, *J. Chem. Phys.* **1969**, *51*, 934.
[49] G. S. Manning, *J. Chem. Phys.* **1969**, *51*, 3249.
[50] T. T. Nguyen, B. I. Shklovskii, *J. Chem. Phys.* **2001**, *114*, 5905.
[51] M. Konieczny, C. N. Likos, *J. Chem. Phys.* **2006**, *124*, 214904.

